Applied Catalysis B: Environmental 213 (2017) 118–126

Contents lists available at ScienceDirect

Applied Catalysis B: Environmental

journal homepage: www.elsevier.com/locate/apcatb

Efficient direct formic acid fuel cell (DFAFC) anode of nano-sized palladium complex: High durability and activity origin

Gumaa A. El-Nagar[a,b,*], Kamal M. Dawood[a], Mohamed S. El-Deab[a,**], Bahgat E. Al-Andouli[a,**]

[a] Department of Chemistry, Faculty of Science, Cairo University, Giza 12613, Egypt
[b] Institut für Chemie und Biochemie Physikalische und Theoretische Chemie, Freie Universität Berlin, 14195, Berlin, Germany

ARTICLE INFO

Article history:
Received 28 February 2017
Received in revised form 25 April 2017
Accepted 2 May 2017
Available online 3 May 2017

Keywords:
Fuel cells
Nano-Pd-Complex
Nanostructured
Electrocatalysis

ABSTRACT

The low stability of Pd-based catalysts extremely obstructs their applied application in the direct formic acid fuel cells (DFAFCs). Herein, a novel nano-sized palladium-complex (nano-$Pd_{complex}$) with outstanding performance (activity and durability) for DFAFCs anodic reaction (Formic acid oxidation; FAO) compared to the commercial Pd-based catalysts is introduced. Morphologically, nano-sized Pd-complex shows an intersected nano-rod like structure with an average particle size ca. 17 nm. Electrochemically, nano-$Pd_{complex}$ modified GC electrode (Nano-$Pd_{complex}$/GC) has 12 times higher electrocatalytic activity, 8.0 times higher electrochemical active surface area, 3.0 times higher catalyst utilization, and ca., 16 times higher stability after 5.0 h than that of traditional Pd nanoparticles modified GC electrode (PdNPs/GC) with the same Pd loading. This significant enhancement in both activity and stability is attributed to nano-$Pd_{complex}$ bulky structure hindering the agglomeration of the Pd active sites and inhibiting the adsorption of poisoning CO-like intermediate species. DFT studies shows that nano-$Pd_{complex}$ has two different geometries: (a) cis-structure which has a square planar geometry and it is inactive for FAO, and (b) trans-structure with a tetrahedral geometry and it is highly active for FAO. This study introduces a new promising category of Pd-based catalyst with high activity, catalyst utilization and durability for DFAFCs applications.

1. Introduction

Fuel cells (FCs) have attracted great research activities over the past few decades owing to the depletion of fossil fuels resources and the ever-increasing of the environmental issues. Thus, direct formic acid fuel cells (DFAFCs) unique features including high theoretical open-circuit potential, sufficiently high energy density, low operating temperatures, non-flammability of formic acid, safe storage and transportation and less crossover of formic acid (FA) through membranes making it an ideal alternative portable power sources for electronic applications (e.g., cell phones, laptops, etc) [1–8]. Pd-based catalysts have commonly been used as excellent anodes for the DFAFCs, generally because of their high catalytic activity and power densities for formic acid oxidation (the essential DFAFCs anodic reaction) compared to Pt-based materials [1,9]. Nevertheless, low stability of the Pd-based catalysts resulting from their poisoning with a strong adsorbed species (e.g., CO) and agglomeration/sintering of Pd active sites has seriously limited their commercial applications [1,9,10]. Thus, many tactics have been developed towards high durability and performance Pd-based catalysts, counting synthesis of Pd with controlled geometry and alloying it with non-precious metals (Co, Ni, Fe, Cu, etc) [11–13]. Even with the huge scientific efforts, the electrocatalytic activity and stability of the used Pd-based catalysts in DFAFCs remains unsatisfactory and needs further improvement, i.e., the development of efficient DFAFCs anode catalyst with a good activity and high stability remains a great challenge towards the commercialization of DFAFCs.

In this regard, this study introduces a novel nano-sized Pd complex catalyst composed of (2-[1-(Benzyloxyimino) ethyl] benzothiazole-κ^2N,N] dichloropalladium(II)) as an efficient and stable alternative electrocatalyst for formic acid electrooxidation (FAO) to the traditional palladium nanoparticles (PdNPs) based catalysts. Physical and electrochemical characterization methods were used to explore the origin of outstanding electrocatalytic activity and stability of as-prepared catalyst. DFT quantum chemi-

* Corresponding author at: Department of Chemistry, Faculty of Science, Cairo University, Giza 12613, Egypt.
** Corresponding authors.
E-mail addresses: Gumaa.elnagar@fu-berlin.de (G.A. El-Nagar), Msaada68@yahoo.com (M.S. El-Deab), bahgat@sci.cu.edu.eg (B.E. Al-Andouli).

http://dx.doi.org/10.1016/j.apcatb.2017.05.006
0926-3373/

cal calculations have been performed to model and characterize the interactions between FA and the Pd-complex. This study presents a new key for the dilemma of the activity and the stability of traditional Pd catalysts based on catalyst design and Pd-complex structure-catalytic activity relationship.

2. Experimental

Glassy carbon (GC, d = 3.0 mm), Ag/AgCl/KCl (sat.), and a spiral Pt wire served as a working, reference and counter electrodes, respectively. GC electrode surface is mechanically polished with aqueous slurries of successively finer alumina powder (down to 0.06 μm), then washed thoroughly with second distilled water and then ethanol. All chemicals used in this work were of analytical grade. They were purchased from Merck and Sigma Aldrich and were used as received without further purification. All solutions were prepared using twice distilled water. Nano-sized Pd complex was prepared and its structure was completely demonstrated as described in our previously published article [14], wherein it used as a precatalyst for synthesis of some organic compounds via Suzuki reactions [14]. Nano-sized Pd-complex modified GC electrode (assigned as nano-$Pd_{complex}$/GC) was prepared as follows: a proper weight of the yellow powder of nano-Pd complex was suspended in 5 ml ethanol and one drop of Nafion solution (5% in water), then the mixture was sonicated for 35 min in an ice bath until a homogenous yellow suspension of Pd-Complex nanostructured is obtained and then various volumes of this suspension were anchored on GC surface in order to prepare electrodes with different nano-$Pd_{complex}$ loadings. On the other hand, Pd nanoparticles (PdNPs) modified GC electrode (next noted as PdNPs/GC) were prepared by electrodeposition from an acidic solution of 0.1 M H_2SO_4 containing 1.0 mM $Pd(CH_3COO)_2$ solution at 0.0 V vs Ag/AgCl for various times which resulted in PdNPs/GC electrode with different PdNPs loadings. The weight of PdNPs was estimated from the amount of charge used for the electrodeposition process.

All measurements are performed at room temperature (25 ± 1 °C) using an EG&G potentiostat (model 273A) operated with Echem 270 software. The electrocatalytic activity of the as-prepared electrodes toward FAO were examined in an aqueous solution of 0.3 M FA. CV was performed in a conventional two-compartment three-electrode glass cell. Electrochemical impedance spectroscopy (EIS) were carried out to characterize the electrochemical properties of the prepared electrodes using an EG&G potentiostat (model 273A) operated with Echem 270 software coupled with lock-in-amplifier used for electrochemical analysis. A field emission scanning electron microscope, FE-SEM, (QUANTA FEG 250) coupled with an energy dispersive X-ray spectrometer (EDX) unit was employed to evaluate the electrode's morphology and surface composition. Current densities were calculated based on the geometric surface area of the working electrodes. Thermogravimetric analysis (TGA using a Shimadzu DTG-60H), FTIR spectra (Pye Unicam SP 3-300), NMR spectra (a Varian Mercury VXR-300 NMR spectrometer at 300 and 75 MHz) were recorded to investigate the change on the Pd-complex structure before and after FAO.

The density functional Theory (DFT) approach has been used to model the interaction of FA with the Pd-complex. All the calculations have been performed using *Gaussian 09* suite of programs [1]. All the geometries were optimized first at HF/3-21G level of theory. The second geometry optimization step was performed using the Density Functional three-parameter hybrid (B3LYP) model by implementing the 6-311++G(d, p) basis set for all the atoms except Pd atom, we used the LanL2DZ basis set. A number of 10 water molecules have been explicitly used in the modeling of the interaction of FA with the Pd-complex. Frequency calculations have been carried out at the same level of theory to characterize the global minima.

3. Results and discussions

3.1. Material, geometrical and electrochemical characterizations

The morphological structure and the composition of the as-prepared catalysts were investigated by FE-SEM and TEM coupled with EDs unit, data are presented in Fig. 1(A–B) and Fig. S1. As clearly seen in Fig. 1A, nano-$Pd_{complex}$ has a homogenously distributed interested nano-rods network structure with average length of ca. 17 nm, while PdNPs (Fig. 1B) shows a sphere-shaped structure with an average particle size of ca. 50 nm. On one hand, EDs analysis qualitatively confirmed the existence of Pd in the both investigated electrodes on the GC surface (see insets of Fig. 1A and B) as evident from the appearance of their constituent elements peak. EDs pattern of the nano-$Pd_{complex}$/GC exhibited peaks for all essential elements of the investigated Pd complex (e.g., Cl (16%), N (6%), C (25%), Pd (23%) and S (10%)), might be suggested and confirmed the existence of the Pd-complex matrix on GC surface before FAO measurements. From the other hand, both of the nano-$Pd_{complex}$ (Fig. 1C-curve b) and PdNPs (Fig. 1C-curve a) modified GC electrodes exhibited the typical characteristic CV of a clean polycrystalline Pd surface in acidic medium, wherein two different regions are observed; Pd surface oxides formation/reduction (≥400 mV) and hydrogen adsorption/desorption peaks ($H_{ads/des}$, ≤ 50 mV)[15,16].

Interestingly, the characteristic CV of the nano-$Pd_{complex}$/GC electrode is very similar to that of metallic palladium, hence one might directly presumed that Pd-complex is decomposed to a certain nice nanostructured pattern of metallic palladium with a significant electrocatalytic activity and stability towards FAO. Actually, this is not the case as revealed from the XRD, FTIR, TGA, AFM and NMR (^1H and ^{13}C) measurements after FAO (see Figs. S2–S7). The obtained complementary information from the above-mentioned techniques are confirmed the stability of the as-prepared Pd-complex under measuring conditions. For instance, FTIR and NMR measuremts after FAO exhibited the existence of all the characteristic functional groups of the studied Pd-complex (Figs. S2 & S3), in addition to its XRD pattern displayed some diffraction peaks for Pd and others for sulfur which both of them are Pd-complex constituent elements (Fig. S4). Moreover, the thermal decomposition measuremts of the Pd-complex after FAO (TGA) showed a four main decomposition stages at 225 °C, 310 °C, 400 °C and 450 °C were attributed to the elimination of CH_2Oph (a mass loss of 22.514%), CH_3CN (mass loss of 9.59%), Cl_2 (mass loss of 15.9%) and palladium residue as a final residue (mass loss of 52%), respectively (Fig. S5), suggesting the existence of Pd-complex matrix on GC surface after FAO, as well. Also, EDs spectrum of the studied Pd-complex exhibited all peaks of its constituent elements before (inset of Fig. 1A) and after (Fig. S6) FAO, in addition, there is no change on the Pd-complex morphological structure before and after FAO investigation as revealed in Fig. S7.

It is worth to mention here that, the nano-$Pd_{complex}$/GC electrode has ca. 8.0 times higher electrochemical active surface area (ECASA) than that of PdNPs/GC electrode with the same Pd loading as estimated from their respective H_{des} peak in Fig. 1C (see inset of Fig. 1C). This may be attributed to the smaller particle size of nano-$Pd_{complex}$ resulting in an increase in the number of corners, edges and defects on the Pd surface (Pd-complex has a higher surface roughness (Ra) compared to PdNPs with the same loading as indicated from AFM, see Fig. S8) leading to higher electrochemical active surface concentration of Pd species.

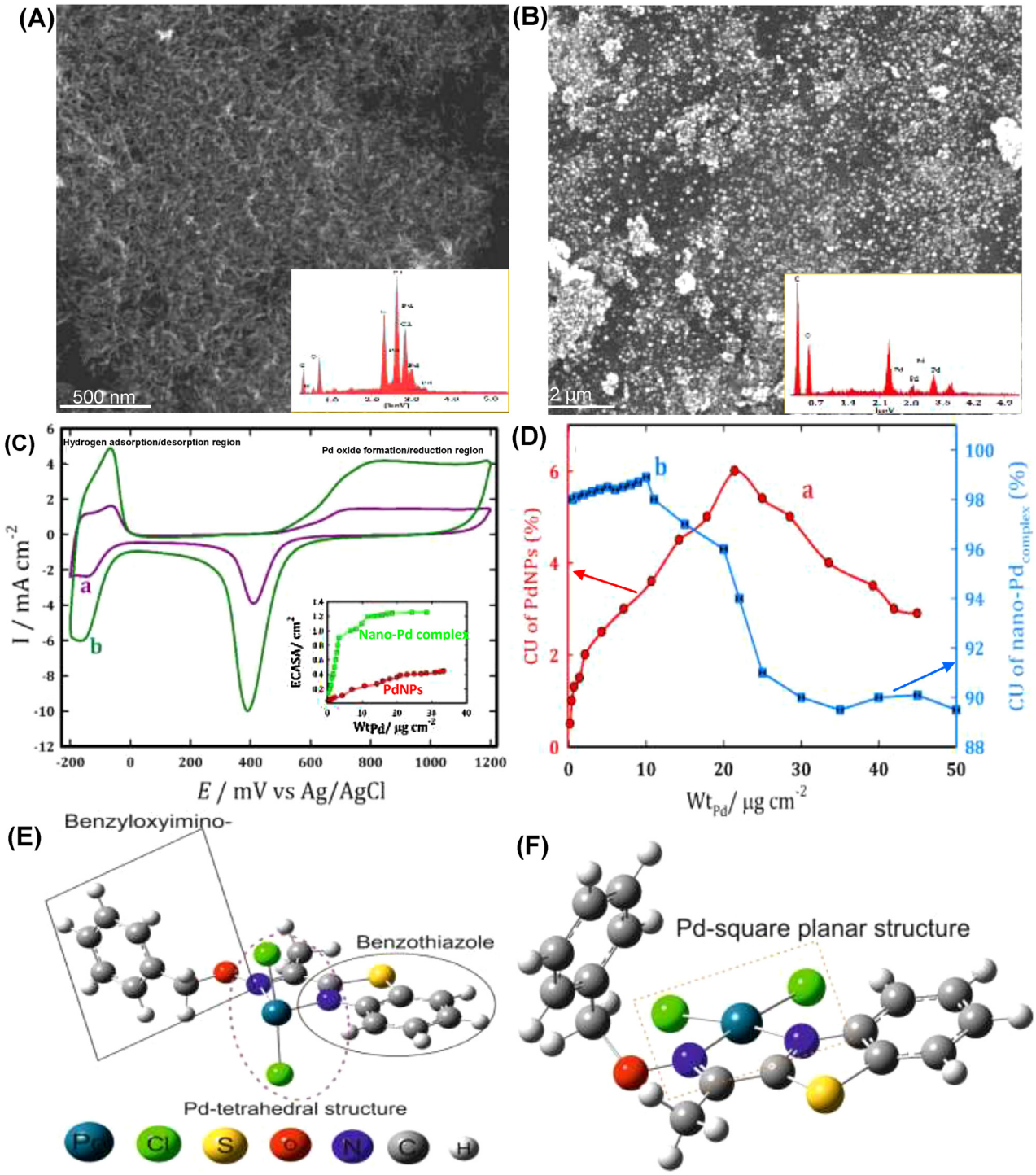

Fig. 1. (A&B) FE-SEM images of nano-$Pd_{complex}$/GC (A) and PdNPs/GC (insets show their respective EDs spectrum), (C) CVs obtained at nano-$Pd_{complex}$/GC (curve b with green color) and PdNPs/GC (curve a with violet color) electrodes in 0.5 M H_2SO_4 with scan rate of 100 mV/s (inset shows the variation of electrochemical active surface area (ECASA) of both electrodes with Pd loading weight (Wt_{Pd})), (D) the variation of catalyst utilization (CU) of nano-$Pd_{complex}$/GC (curve b in blue color) and PdNPs/GC (curve a in red color) with Wt_{Pd} and (E&F) the two different optimized structure of nano-$Pd_{complex}$ (namely, (E) trans-geometry and (F) cis-geometry) calculated at the B3LYP/6-311++G(d, p)/LanL2DZ level of theory. (For interpretation of the references to colour in this figure legend, the reader is referred to the web version of this article.)

The cost of FCs catalysts is a key parameter obstructing the FC world-wide commercialization. Generally, using a higher catalyst loading leads to a better performance, but unfortunately with higher cost. Therefore, one of the main targets in FCs development is how to reduce the catalyst loading without sacrificing the FCs performance and durability. Consequently, a function called catalyst utilization (CU) was provided in order to probe the catalyst effective surface area. CU is the ratio between Pd electrochemical active surface area which accessible for electrons (calculated using amount of charge under $H_{ads/des}$ peak using the well-established standard value of 0.21 µc/cm^2) to the total Pd surface area (estimated using the Pd loading, density and average particle size)[17–19], data are presented in Fig. 1D. As revealed in this figure, while more than 90% of the nano-$Pd_{complex}$/GC electrode (curve b) is active surface

area for FAO, only 6% of PdNPs/GC electrode is active surface area for FAO. One might be safely argued that CU of nano-$Pd_{complex}$/GC electrode is ca., 16 times higher than that of PdNPs/GC electrode with the same Pd weigh.

DFT calculations were used primarily to optimized the nano-Pd complex structure at the B3LYP/6-311++G(d,p)/LanL2DZ level of theory. Nano-Pd-complex showed two minimum optimized structures; namely cis-structure (Fig. 1E) and trans-structure (Fig. 1F). As shown in Fig. 1E, the Pd atom of cis-structure forms a square planar geometry, where the two chlorine atoms located in the cis-position and have almost the same bond length. In addition, the two Pd-N bonds of the five-membered ring have identical bond length (2.1 Å). From the other hand, trans-structure (Fig. 1F) exhibits a distorted tetrahedral structure, where the two chlorine atoms are located in the trans-position. The two Pd-N bonds length of the five-membered ring are not identical, one of them is 2.7 Å and the other one is 2.01 Å.

3.2. Electrocatalytic activity: formic acid electrooxidation (FAO)

Fig. 2A shows CVs of FAO obtained at the PdNPs/GC (curve a, Wt_{Pd} = 20 μg/cm^2) and nano-$Pd_{Complex}$/GC with different Pd loadings (typically; b) 5, (c) 10, (d) 15 and (e) 20 μg/cm^2) electrodes in 0.3 M FA aqueous solution. As clearly seen in this figure, both nano-$Pd_{complex}$/GC and PdNPs/GC (curve a) electrodes exhibited the typical CVs of FAO at Pd-based catalysts. Interestingly, nano-$Pd_{complex}$/GC electrode (curve e) displays ca. 12 times higher electrocatalytic activity towards FAO compared to PdNPs/GC electrode (curve a) with the same Pd weight, as calculated using the amount of charge associated with FAO in both cases. In addition to, a significant negative shift in FAO onset potential (ca., 150 mV) indicating the faster kinetic of FAO at nano-$Pd_{complex}$ compared to PdNPs. This dramatic enhancement might be attributed to the electronic and surface enhancement of the smaller particle size associated with the environment surrounding the active Pd sites of the Pd-complex. However, nano-$Pd_{complex}$/GC electrode has ca., 8.0 times higher active surface area compared to that of PdNPs/GC electrode, it exhibits ca. 12 times higher electrocatalytic activity compared to the PdNPs/GC electrode (curve a), despite of using equal Pd loading. The suitable explanation for this observation is the low coordinate number of Pd atom in the complex allows Pd to attach more than one FA molecule via a strong binding between the FA and the active Pd sites after replacing the Cl ligands, initiating the oxidation reaction, beside the bulky structure of Pd-complex could resist the accumulation of poisoning intermediates such as CO, which is produced from the "*non-faradic*" dissociation of FA at Pd surface. Inset of Fig. 2A shows the variation of the amount of charge consumed during the direct FAO (Q_{FAO}) at nano-$Pd_{complex}$/GC (curve b) and PdNPs/GC electrode (curve a) as a function of Pd loadings (Wt_{Pd}). As shown in this figure, Q_{FAO} of nano-$Pd_{complex}$/GC increases sharply with the nano-$Pd_{complex}$ loading increasing and then it levels off at $Pd_{complex}$ loading equals ~15 μg/cm^2.

The same behavior is obtained at PdNPs/GC electrode. Remarkably, nano-$Pd_{complex}$/GC electrode has a significantly higher electrocatalytic activity for FAO compared to PdNPs/GC electrode over the entire studied Pd loading weight range (see inset of Fig. 2A). For example, nano-$Pd_{complex}$/GC electrode exhibited ca. 12 times higher electrocatalytic activity towards FAO than PdNPs/GC electrode at Pd weight of 5 μg/cm^2.

Another important enhancement index namely atom economy of the catalyst (AE) probing the incorporated proportion of Pd atoms into the direct oxidation of FA to CO_2 (i.e., FAO oxidation efficiency). AE is defined as the number of Pd atoms incorporated in FAO (was estimated using the Q_{FAO} and with the assumption that 1 cm^2 of Pd surface contains ca. 1.5×10^{15} atoms) divided by the total number of Pd atoms (as calculated using amount of charge under the H_{des} peak)[20,21]. Fig. 2B shows the variation of AE of PdNPs/GC (curve a) and nano-$Pd_{complex}$/GC (curve b) electrodes as a function of Wt_{Pd}. As seen in this figure, while more than 97% of the Pd atoms of nano-$Pd_{complex}$/GC electrode (curve b) are incorporated into FAO process, only 45% of the PdNPs/GC electrode (curve a) Pd atoms are participated in FAO with $Wt_{Pd} \leq 20\ \mu g\ cm^{-2}$. Beyond this weight AE of nano-$Pd_{complex}$/GC electrode approximately 83% compared to only 21% for PdNPs/GC electrode. That is, nano-$Pd_{complex}$/GC electrode is at least 2.0 times more efficient for FAO compared to the PdNPs/GC electrode with the same Pd weight. Closer examination of Fig. 2A and B shows that, the number of Pd atoms (active sites) incorporated into FAO for nano-$Pd_{complex}$/GC electrode is 2.0 times higher compared to that value of PdNPs/GC electrode as long as $Wt_{Pd} \leq 20\ \mu g\ cm^{-2}$, however the electrocatalytic activity of nano-$Pd_{complex}$/GC electrode is 12 times higher compared to PdNPs/GC electrode as estimated from FAO current density. This might be explained insight of each Pd atom in nano-$Pd_{complex}$/GC electrode is active for more than one FA molecules (i.e., Pd complex has a high FA coordination capacity). i.e., the low coordination number of the studied Pd-complex allows more than one FA molecule attached to the same Pd active center, indicating the proposed Pd-complex has a high coordination capacity which allowing oxidation more than one FA molecules at the same Pd site.

The charge transfer performance of PdNPs and nano-$Pd_{complex}$ modified GC electrodes, is one of the key parameter to evaluate their electrocatalytic activity, was further investigated by electrochemical impedance spectroscopy (EIS). Fig. 2C shows the Nyquist plots of PdNPs/GC (curve a, $Wt_{Pd} = 5\ \mu g\ cm^{-2}$) and nano-$Pd_{complex}$/GC with different Pd loadings (curves b-e) catalysts measured in 0.3 M FA. The semicircle diameter in a Nyquist plot reveals the charge transfer resistance of the reactions. Smaller diameter indicates lower charge transfer resistance for the reaction and higher electrocatalytic activity. Zview software was used to fit the impedance data and equivalent circuit was also displayed in Fig. 2C. This figure reveals that, nano-$Pd_{complex}$/GC electrode (curve b) exhibited a much smaller FAO charge transfer resistance than that of PdNPs/GC electrode (curve a) with the same Pd weight. In addition to, the charge transfer resistance of nano-$Pd_{complex}$/GC electrode decreased with the increase in the nano-Pd complex weight (curves b–e). This results are suggesting the superior electrical conductivity of nano-$Pd_{complex}$ and indicating the faster charge-transfer kinetics of FAO at nano-$Pd_{complex}$ compared to PdNPs/GC electrode. This may be attributed to the bulky structure of Pd-complex which hinders the adsorption of the poisoning intermediates (e.g., CO) on the Pd active sites, in addition to prevent the aggregation/dissolution of the Pd active sites.

The stability of Pd-based catalysts towards FAO is a major challenge hindering their practical applications in DFAFCs. Consequently, the stability of the proposed Pd-complex catalyst was next investigated using chronoamperometry method, data presented in Fig. 2D. This figure shows the current transient plots of PdNPs/GC (curve a, $Wt_{Pd} = 10\ \mu g\ cm^{-2}$), nano-$Pd_{complex}$/GC (curve b, $Wt_{Pd} = 5\ \mu g\ cm^{-2}$) and nano-$Pd_{complex}$/GC (curve c, $Wt_{Pd} = 10\ \mu g\ cm^{-2}$) electrodes in 0.3 M FA. As clearly seen in this figure, nano-$Pd_{complex}$/GC electrodes (curves b&c) support higher FA oxidation current and higher stability compared to the traditional PdNPs/GC electrode (curve a). For instance, PdNPs/GC electrode electrocatalytic activity for FAO decreased by 95% after only half hour (curve a), while the activity of nano-$Pd_{complex}$/GC electrode with same Pd weight (curve c) decreased only by 5%, i.e, nano-$Pd_{complex}$/GC electrode exhibited 19 times higher stability compared to traditional PdNPs modified GC electrode with the same Pd loading. The fast decay of FAO current density at PdNPs/GC electrode (with estimated poisoning rate of 0.1% s^{-1}) may be ascribed to accumulation of PdNPs and/or deactivation of active PdNPs sites with a highly adsorbed species (e.g., CO, hydro-

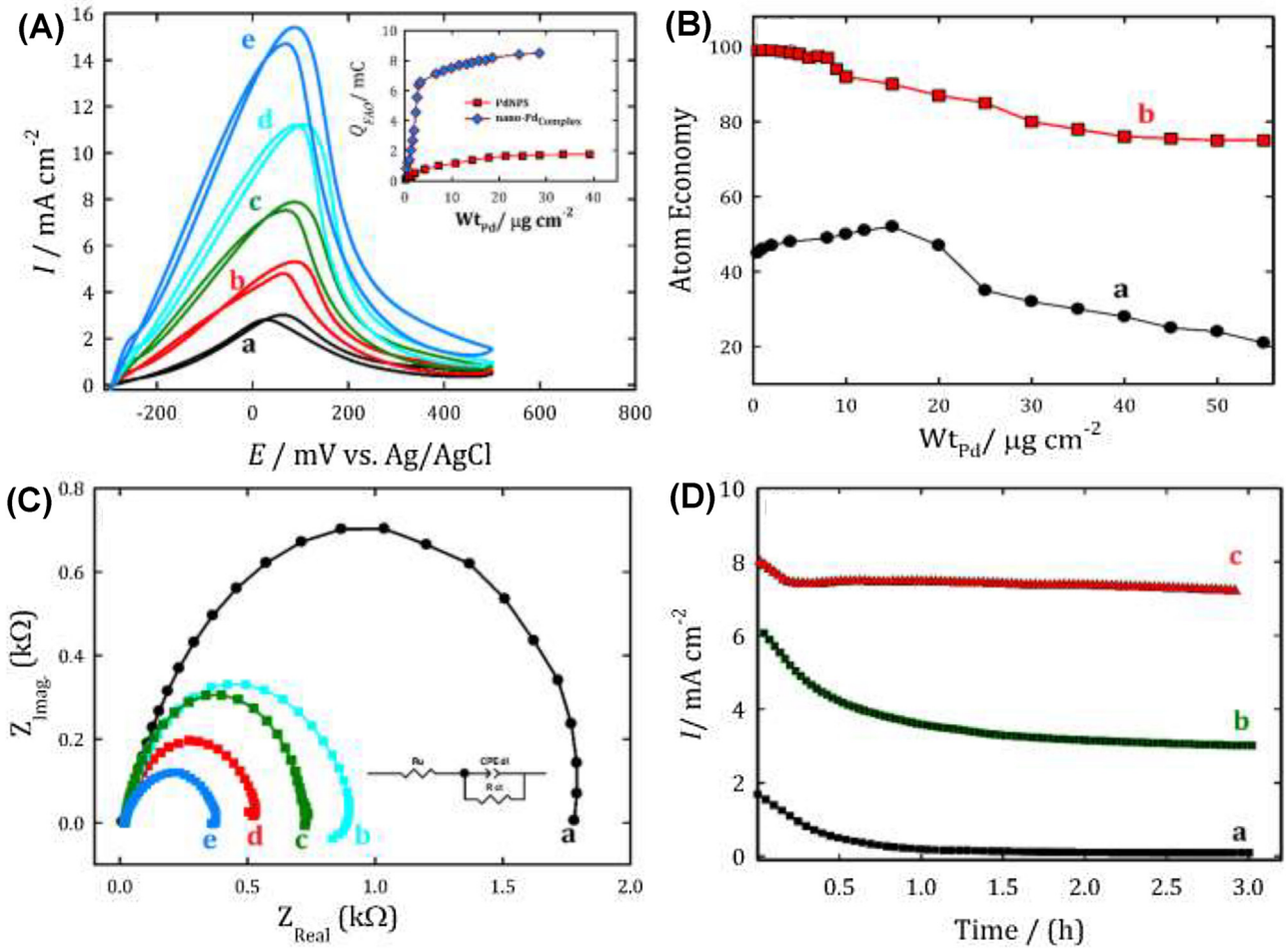

Fig. 2. (A) CVs obtained at PdNPs/GC (curve a, WtPd ~ 20 μg/cm^2) and nano-Pd$_{Complex}$/GC with various Pd loadings (curves b–e; typically, (b) 5, (c) 10, (d) 15 and (e) 20 μg/cm^2) in 0.3 M FA aqueous solution (inset shows the variation of the amount of charge associated with FAO (Q_{FAO}) as a function in Wt$_{Pd}$), (B) the variation of atom economy index (AE) of PdNPs/GC (curve a) and nano-Pd$_{Complex}$/GC (curve b) as a function in Wt$_{Pd}$, (C) Nyquist plots of PdNPs/GC (curve a, WtPd ~ 20 μg/cm^2) and nano-Pd$_{Complex}$/GC with various Pd loadings (curves b–e; typically, (b) 5, (c) 10, (d) 15 and (e) 20 μg/cm^2) and (D) current transient (i-t) measurements of PdNPs/GC (curve a, WtPd ~ 20 μg/cm^2) and nano-Pd$_{Complex}$/GC with two different loadings (typically, (b) 5 μg/cm^2 and (c) 10 μg/cm^2).

carbon impurities). Controversy, the nano-Pd$_{complex}$/GC electrode supports at least 16 times higher FAO current after long continuous electrolysis and has a slower current decay rate (with a calculated poisoning rate of 0.001% s^{-1}). These findings support our assumption that, the enhancement in the catalytic stability is attributed to a significant role of the bulky structure of Pd-complex and the Pd-complex matrix is very stable under the measuring conditions. The complex acts as a "shell" in protecting the PdNPs as a "core" from the mechanical detachment at the electrode's surface possibly via preventing/inhibiting the embrittlement of Pd and/or improving their electronic properties.

3.3. Activity and durability origin of Pd-complex

Generally, the performance degradation of the traditional Pd-based anodes is attributed to the adsorption of poisoning intermediates such as CO and/or the agglomeration/sintering of Pd nanoparticles which resulted in a significant decrease in the active surface area. In this regard, FE-SEM (Fig. 3) and CVs (Fig. 4) of the as-prepared catalysts were investigated at various FAO stages, in order to observe any physical change such as sintering of Pd active sites, active surface area and morphology changes during the reaction. As seen in Fig. 3(A–C), there is no observable agglomeration for the nano-Pd-complex nanoparticles and no significant change in its morphology before and after 1 and 3 h of continuous electrolysis in FA solution. There is no change in its active surface area and no CO accumulation is observed as well (Fig. 4A), indicating the high stability of our proposed catalyst (nano-Pd-complex). In contrast, FE-SEM images of the traditional PdNPs before and after FAO showed the aggregation of the PdNPs (Fig. 3(D–F)). Additionally, its electrochemical active surface area is significantly decreased (e.g., ECASA reduced by 40%, 60% and 75% after 1,2 and 3 h of continuous FAO, respectively, Fig. 4B) might be due to the accumulation or dissolution of PdNPs and/or poisoning with CO-like adsorption as indicated from the appearance of broad peak around 0.65 V attributed to CO oxidation (Fig. 4B). From the other hand, FA charge transfer resistance of PdNPs catalyst significantly increased with increasing FAO electrolysis time (Fig. 4D). This might be attributed to the aggregation/dissolution of PdNPs and/or deactivated of PdNPs surface with CO adsorption. Interestingly, the charge transfer resistance of FA at nano-Pdcomplex catalyst didn't changed before and after 3 h of FA continuous electrolysis (Fig. 4C).

It worth to mentioned here that, our proposed catalyst exhibits a higher electrocatalytic activity and stability compared the commercial Pd/C (20%) with the same palladium loading weight (see Fig. S9). For instance, our proposed catalyst (nano-sized Pd-complex) supported ~1.8 times higher electrocatalytic activity together with ~200 mV negative shift of formic acid oxidation onset potential (See Fig. S9A). In addition, the commercial Pd/C lost about 66% from its original activity compared to only 5.4% of the nano-sized Pd

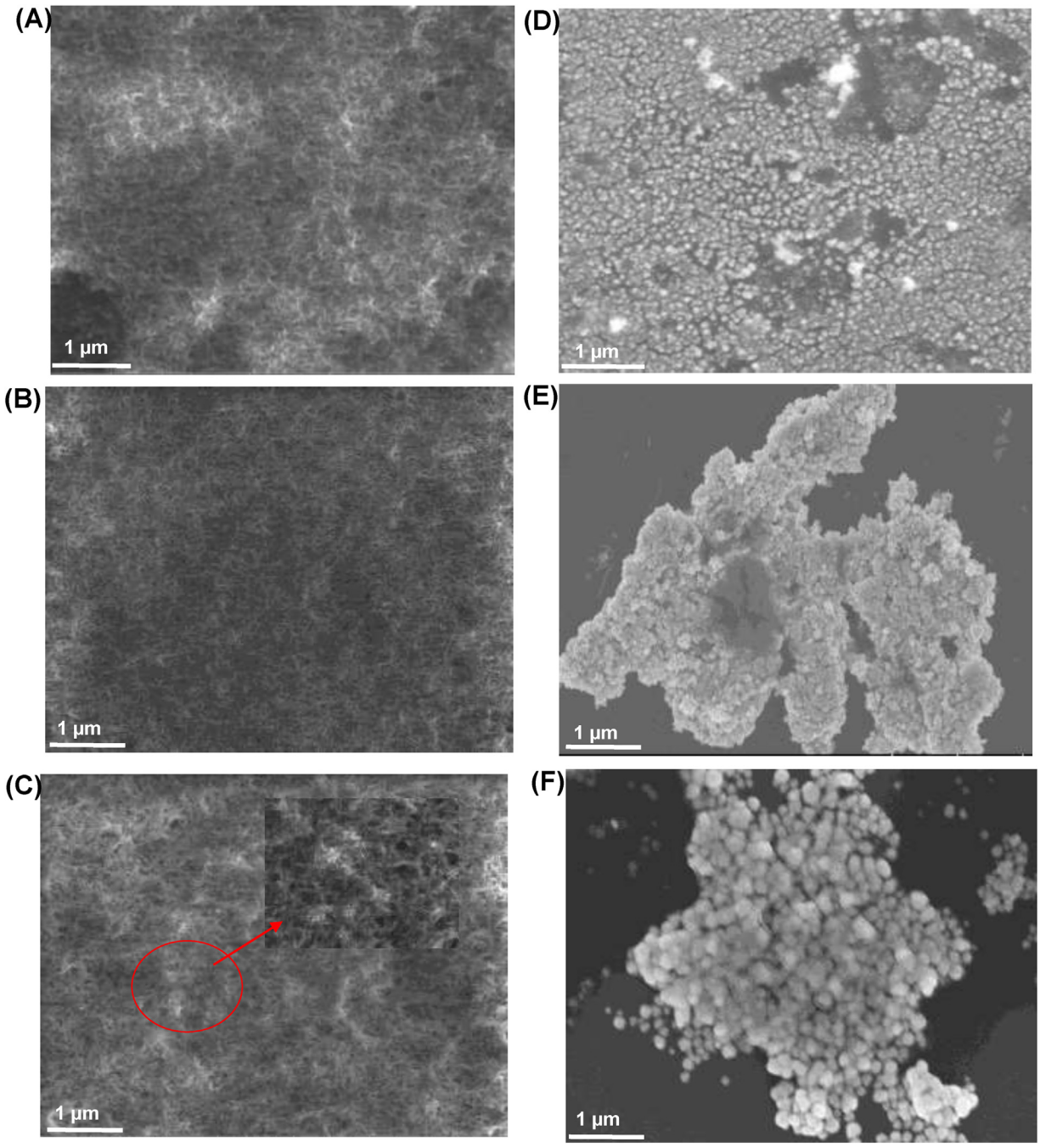

Fig. 3. FE-SEM images of nano-$Pd_{complex}$/GC (A–C) and PdNPs/GC (D–F) electrodes before (A & D) and after 1.0 (B & E) and 3.0 (C & F) of continuous formic acid electrolysis.

complex after 1.0 h of continuous formic acid electrolysis (See Fig. S9B).

In summary, PdNPs catalysts deactivation is caused by two different mechanisms: (a) surface poisoning of the Pd catalyst with CO-like species and (b) aggregation/dissolution of the Pd catalyst particles. Note that, the reactivation process can recover cell performance that has been deactivated by surface poisoning, but the performance degradation caused by particle aggregation/dissolution cannot be recovered. This means that aggregation between the catalyst particles is a serious problem over the life of the FCs. The high activity and stability of our proposed catalyst compared to traditional Pd-based catalyst is attributed to its bulky structure which prevent preventing its aggregation and resisting CO poisoning. Additionally, it has a high active surface area and catalyst utilization compared with PdNPs catalyst.

3.4. DFT calculations

DFT calculations have been performed to investigate the interactions of FA and/or CO with Pd-complex catalyst and to correlate the Pd-complex electrocatalytic activity with its structure (Fig. 5). Firstly, the two different Pd-complex geometries (namely, cis-structure and trans-structure) were optimized in the presence of nine water molecules (data not shown). In both cases, water molecules form a well-defined H-bond network with each other (forming a bilayer of vertical and horizontal water molecules) and one water molecule replaced one of the Cl ligands forming bond

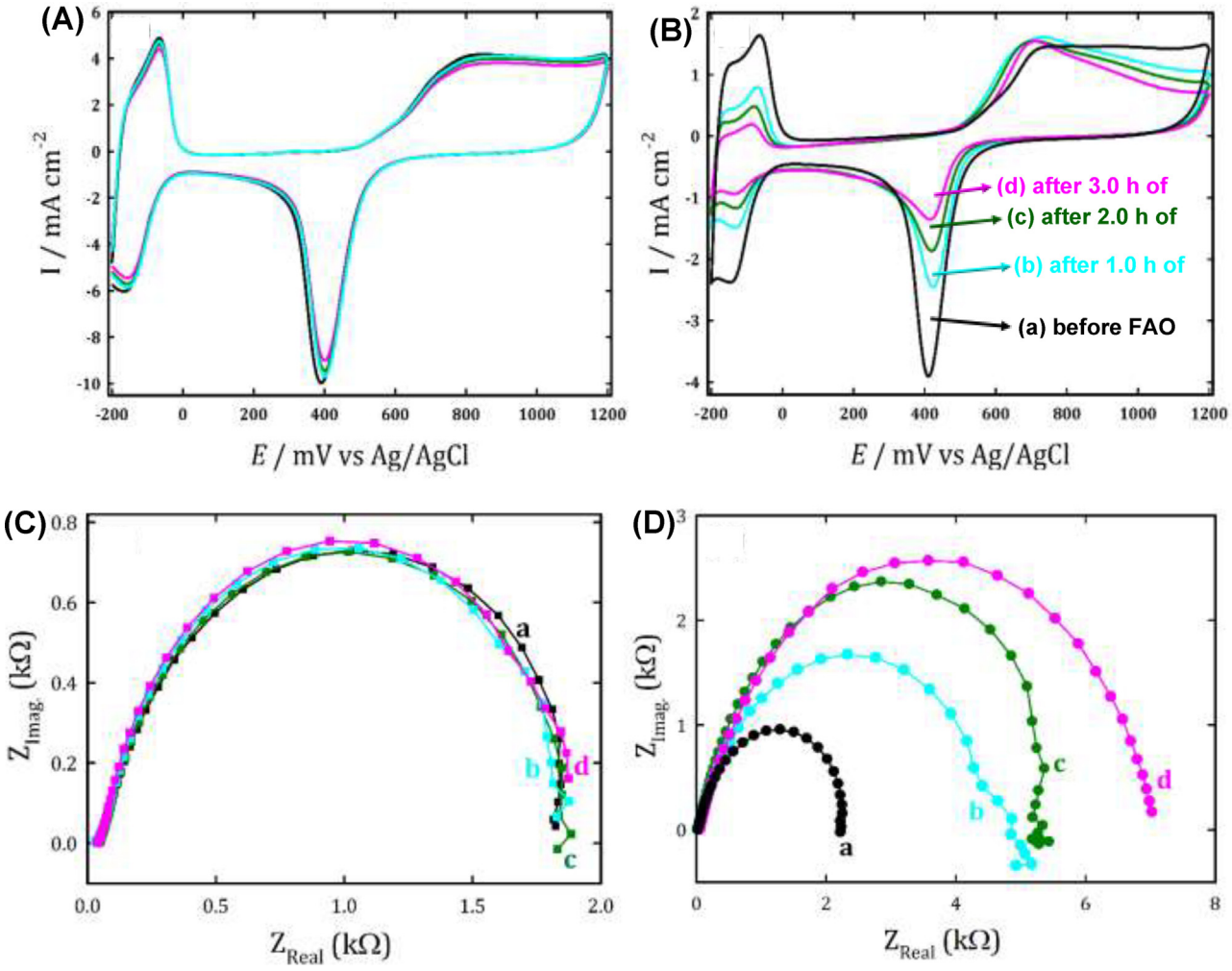

Fig. 4. CVs obtained at (A) nano-$Pd_{complex}$/GC and (B) PdNPs/GC electrodes in 0.5 M H_2SO_4 before (black line (curve a) in each plot) and after various time of continuous FAO electrolysis (colored lines in each plot, typically; (b) 1 h, (c) 2 h and (d) 3 h) and (C&D) Nyquist plot of nano-$Pd_{complex}$/GC (C) and PdNPs/GC (D) electrodes (same colors and notations are used as in Fig. 4(A&B)).

with the Pd atom (Pd—O bond, bond length ~2.058 Å) in the case of trans-structure. Moreover, the tetrahedral structure of trans-form is converted to square planar structure. On the other hand, there is no bond is formed between the water molecules and cis-form of Pd-complex. Interestingly, the addition of one FA molecule to the trans-structure of Pd-complex resulted in a formation of a new bond between oxygen atom of FA carbonyl group and Pd atom in the complex with a Pd—O bond length of 2.045 Å, besides the O—H bond of the adsorbed FA is lengthened to 1.44 Å, which is 0.465 Å longer than that in the free FA molecule and the C—H bond remains almost the same, forming a formate intermediate attached to the Pd site. Additionally, the Pd keeps its square planar structure as in the case of water alone. From the other hand, no interaction (no bond formed between FA and Pd) is observed between FA molecule and the solvated cis-structure of Pd-complex which has a square planar structure from the beginning (Fig. 5B). That is, cis-form of Pd complex (with square planar structure) is in active for FA oxidation, while trans-form with tetrahedral structure is highly active for FA oxidation. Further addition of one CO to the trans-model system (N.b., CO and FA located at the same distance from the Pd active site, Fig. 5C). As shown in this figure, there is no interactions between the Pd and CO is observed, while a bond between the carbonyl oxygen of FA and Pd atom is formed and CO moved far away from the Pd site. A stronger Pd—O bond of 1.95 Å is formed and the C—H bond of the adsorbed HCOOH is elongated to 1.18 Å instead of 1.10 Å in the free HCOOH. In addition, the OH bond is elongated to 1.05 Å instead of 0.965 Å in the free HCOOH molecule. Interestingly, when the CO is put at a closer distance to Pd active site than FA molecule (Fig. 5D), the two molecules (CO and FA) are formed bond with the Pd active site via elimination of one Pd—Cl bond and broken one of Pd—N five membered ring bond, indicating that the higher CO tolerance of the nano-Pd-complex. These findings support the argument that the complex as a shell protects and/or keep the Pd (i.e. the active site) with lower coordinate number, allowing for effective interaction with FA. Even if CO is formed, the Pd active center will still active for FA adsorption and oxidation as evidenced from Fig. 5D. When one CO molecule are allowed to interact with the two different geometries of the Pd-complex in presence of H_2O. There is no bond formed between Pd and CO molecule in the both cases rather it preferred to coordinate with H_2O instead of CO in the case of trans-Pd complex structure (data not shown).

Now, we are trying to design a new catalyst based on the obtained results herein via studying the effect of introducing various donating (e.g., NH2, OH, etc) and withdrawing (e.g., COOH, NO2) functional groups on the nano-sized Pd complex structure, activity and durability. In addition, we will do our best to study the formic acid single molecule (non-fluorescent molecule) electrocatalysis (SMECNFM) on our proposed and the new designed nano-Pd complex catalysts by coupling SMECNFM with a single

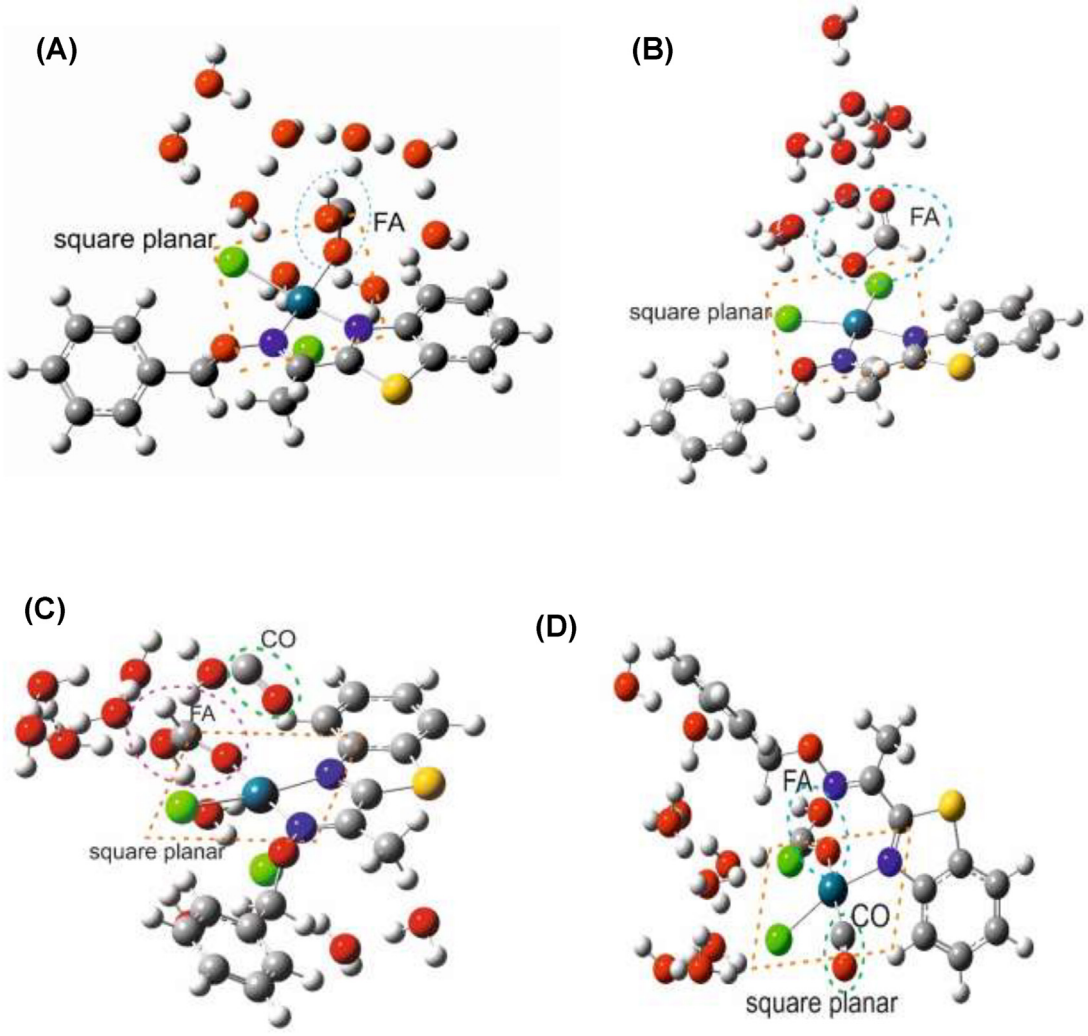

Fig. 5. DFT optimized structures of solvated trans-Pd-complex (A) and cis-Pd-complex (B) in the presence of 9 water molecules and 1 FA molecule, (C) solvated trans-Pd-complex in existence of CO, FA and water molecules (FA and CO were located at same distance from Pd-complex) and (D) the same of model (C) but CO was located closer to the Pd-complex.

molecule fluorescence reaction. This method is innovated by Fei-Fei Li et al. [22].

4. Conclusions

This study introduces a novel nano-sized Pd-complex catalyst (nano-$Pd_{complex}$) with outstanding electrocatalytic activity, CO tolerance and excellent stability towards FAO compared to the traditional PdNPs catalysts. Nano-$Pd_{complex}$ exhibited 8.0 times higher electrochemical active surface area, 12 times higher electrocatalytic activity, 3 times higher catalyst utilization and 16 times higher stability compared to the traditional PdNPs for FAO.

The high activity of nano-$Pd_{complex}$ is attributed to its high coordination capacity and smaller particle size and its excellent stability is attributed to its bulky structure preventing its agglomeration/sintering and resisting CO accumulation on its surface. On the other hand, the poor durability of the traditional PdNPs catalysts is due to the accumulation of CO-like intermediates and/or the aggregation of the Pd particles which resulted in significant decrease in its active surface area. DFT calculations showed that Pd-complex has two different geometries; namely cis-form with square planar geometry and trans-form with tetrahedral geometry. Cis-Pd complex is inactive for FAO, while trans-Pd complex is highly active for FAO. Trans-Pd complex structure act as shell providing Pd active sites for interaction with FA and prevent poisoning by CO adsorption and Pd aggregation.

Appendix A. Supplementary data

Supplementary data associated with this article can be found, in the online version, at http://dx.doi.org/10.1016/j.apcatb.2017.05.006.

References

[1] G.A. El-Nagar, A.F. Darweesh, I. Sadiek, Electrochim. Acta 215 (2016) 334–338.
[2] O.Z. Sharaf, M.F. Orhan, Renew. Sustain. Energy Rev. 32 (2014) 810–853.
[3] Y. Wang, K.S. Chen, J. Mishler, S.C. Cho, X.C. Adroher, Appl. Energy 88 (2011) 981–1007.
[4] C. Rice, S. Ha, R.I. Masel, P. Waszczuk, A. Wieckowski, T. Barnard, J. Power Sources 111 (2002) 83–89.
[5] A.M. Mohammad, G.A. El-Nagar, I.M. Al-Akraa, M.S. El-Deab, B.E. El-Anadouli, Int. J. Hydrogen Energy 40 (2015) 7808–7816.
[6] J. Joo, M. Choun, J. Jeong, J. Lee, ACS Catal. 5 (2015) 6848–6851.
[7] Z. Bai, L. Yang, L. Li, J. Lv, K. Wang, J. Zhang, J. Phys. Chem. C 113 (2009) 10568–10573.
[8] X. Yu, P.G. Pickup, J. Power Sources 182 (2008) 124–132.
[9] M. Ren, Y. Kang, W. He, Z. Zou, X. Xue, D.L. Akins, H. Yang, S. Feng, Appl. Catal. B: Environ. 104 (2011) 49–53.
[10] X. Yu, P.G. Pickup, Electrochem. Commun. 11 (2009) 2012–2014.
[11] R. Wang, H. Wang, X. Wang, S. Liao, V. Linkov, S. Ji, Int. J. Hydrogen Energy 38 (2013) 13125–13131.

[12] F. Yang, Y. Zhang, P.-F. Liu, Y. Cui, X.-R. Ge, Q.-S. Jing, Int. J. Hydrogen Energy 41 (2016) 6773–6780.
[13] B. Yu, W. Wen, W. Li, Y. Yang, D. Hou, C. Liu, Electrochim. Acta 196 (2016) 223–230.
[14] A.F. Darweesh, M.R. Shaaban, A.M. Farag, P. Metz, K.M. Dawood, Synthesis 2010 (2010) 3163–3173.
[15] R. Yue, C. Wang, F. Jiang, H. Wang, Y. Du, J. Xu, P. Yang, Int. J. Hydrogen Energy 38 (2013) 12755–12766.
[16] J. Bai, L. Shen, D. Sun, Y. Tang, T. Lu, CrystEngComm 16 (2014) 10445–10450.
[17] F.-C. Wu, C.-C. Wan, Y.-Y. Wang, L.-D. Tsai, K.-L. Hsueh, J. Electrochem. Soc. 154 (2007) B528–B532.
[18] K.R. Cooper, Fuel Cell Mag. 9 (2009).
[19] D.P. Wilkinson, J. Zhang, R. Hui, J. Fergus, X. Li, Proton Exchange Membrane Fuel Cells: Materials Properties and Performance, CRC Press, 2009.
[20] G.A. El-Nagar, A.M. Mohammad, M.S. El-Deab, T. Ohsaka, B.E. El-Anadouli, J. Power Sources 265 (2014) 57–61.
[21] G.A. Somorjai, Y. Li, Introduction to Surface Chemistry and Catalysis, John Wiley & Sons, John Wiley & Sons, 2010.
[22] F.-F. Li, J.-N. Gu, X.-C. Zhou, Chin. Chem. Lett. 26 (2015) 1514–1517.